AFRL-RY-WP-TR-2012-0338

QUANTUM DOT DETECTOR ENHANCEMENT FOR NARROW BAND MULTISPECTRAL APPLICATIONS

John S. Derov and Neda Mojaverian

Infrared Technology Branch
Electromagnetics Technology Division

OCTOBER 2012
Interim Report

AIR FORCE RESEARCH LABORATORY
SENSORS DIRECTORATE
WRIGHT-PATTERSON AIR FORCE BASE, OH 45433-7320
AIR FORCE MATERIEL COMMAND
UNITED STATES AIR FORCE

NOTICE AND SIGNATURE PAGE

Using Government drawings, specifications, or other data included in this document for any purpose other than Government procurement does not in any way obligate the U.S. Government. The fact that the Government formulated or supplied the drawings, specifications, or other data does not license the holder or any other person or corporation; or convey any rights or permission to manufacture, use, or sell any patented invention that may relate to them.

This report was cleared for public release by the USAF 88th Air Base Wing (88 ABW) Public Affairs Office (PAO) and is available to the general public, including foreign nationals. Copies may be obtained from the Defense Technical Information Center (DTIC) (http://www.dtic.mil).

AFRL-RY-WP-TR-2012-0338 HAS BEEN REVIEWED AND IS APPROVED FOR PUBLICATION IN ACCORDANCE WITH ASSIGNED DISTRIBUTION STATEMENT.

*//Signature//

JOHN S. DEROV
Program Manager
Infrared Sensor Technology Branch
Electromagnetics Technology Division

//Signature//

MARK G. SCHMITT, Chief
Infrared Sensor Technology Branch
Electromagnetics Technology Division

//Signature//

DANE F. FULLER, USAF, Lt Col
Division Chief
Electromagnetics Technology Division
Sensors Directorate

This report is published in the interest of scientific and technical information exchange and its publication does not constitute the Government's approval or disapproval of its ideas or findings.

*Disseminated copies will show "//Signature//" stamped or typed above the signature blocks.

REPORT DOCUMENTATION PAGE

Form Approved
OMB No. 0704-0188

1. REPORT DATE *(DD-MM-YY)*	2. REPORT TYPE	3. DATES COVERED *(From - To)*
October 2012	Interim	1 October 2010 – 1 October 2012

4. TITLE AND SUBTITLE
QUANTUM DOT DETECTOR ENHANCEMNT FOR NARROW BAND MULTISPECTRAL APPLICATIONS

5a. CONTRACT NUMBER
In-house

5b. GRANT NUMBER

5c. PROGRAM ELEMENT NUMBER
61102F

6. AUTHOR(S)
John S. Derov and Neda Mojaverian

5d. PROJECT NUMBER
3001

5e. TASK NUMBER
11

5f. WORK UNIT NUMBER
Y00K

7. PERFORMING ORGANIZATION NAME(S) AND ADDRESS(ES)
Infrared Technology Branch
Electromagnetics Technology Division
Air Force Research Laboratory, Sensors Directorate
Wright-Patterson Air Force Base, OH 45433-7320
Air Force Materiel Command, United States Air Force

8. PERFORMING ORGANIZATION REPORT NUMBER
AFRL-RY-WP-TR-2012-0338

9. SPONSORING/MONITORING AGENCY NAME(S) AND ADDRESS(ES)
Air Force Research Laboratory
Sensors Directorate
Wright-Patterson Air Force Base, OH 45433-7320
Air Force Materiel Command
United States Air Force

10. SPONSORING/MONITORING AGENCY ACRONYM(S)
AFRL/RYHI

11. SPONSORING/MONITORING AGENCY REPORT NUMBER(S)
AFRL-RY-WP-TR-2012-0338

12. DISTRIBUTION/AVAILABILITY STATEMENT
Approved for public release; distribution unlimited

13. SUPPLEMENTARY NOTES
PAO case number 88ABW-2012-6040; Clearance Date 16 November 2012. Report contains color.

14. ABSTRACT
This is a work of the U.S. Government and is not subject to copyright protection in the United States. The underlying principle of a photodetector is converting the optical signal into electrical signal. Under the radiation of an optical field, excess carriers are generated from the active region in the semiconductor, the electrons in conduction band and the holes in valence band. The increase of electron-hole pairs is bonding to the variation of the physical parameters. By analyzing the physical parameters through associated circuitry or systems, the characteristic of the incident photons can be identified.

15. SUBJECT TERMS
Quantum Dot, Quantum Well, Photodetectors

16. SECURITY CLASSIFICATION OF:			17. LIMITATION OF ABSTRACT:	18. NUMBER OF PAGES	19a. NAME OF RESPONSIBLE PERSON (Monitor)
a. REPORT	b. ABSTRACT	c. THIS PAGE			John S. Derov
Unclassified	Unclassified	Unclassified	SAR	30	19b. TELEPHONE NUMBER *(Include Area Code)* N/A

TABLE OF CONTENTS

SECTION **PAGE**

LIST OF FIGURES

1. Introduction – Photodetectors

A photodetector is a specific semiconductor device which is capable of detecting the existence of incident photons [1]. Different from thermal detector that mainly responses to the heating effect of the optical radiation, photodetector is able to sensing the light by direct interaction between the optical energy and the semiconductor material.

The underlying principle of a photodetector is converting the optical signal into electrical signal. Under the radiation of an optical field, excess carriers are generated from the active region in the semiconductor, the electrons in conduction band and the holes in valence band [2]. The increase of electron-hole pairs is bonding to the variation of the physical parameters. By analyzing the physical parameters through associated circuitry or systems, the characteristic of the incident photons can be identified.

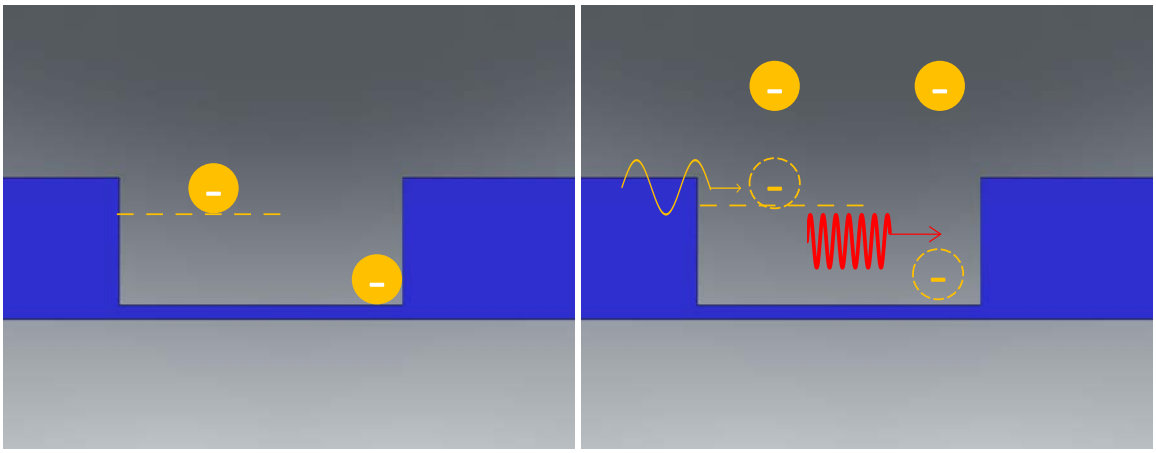

Figure 1: Photodetection Process

Figure 1 illustrates the working mechanism for the photo detecting process. Before the photon flux incident on the material, the electrons in the p-n junction cannot make any contribution to the electric current, either because that they were blocked by the potential barrier, or is trapped by a bound state. Only if the electron was excited by the photons with enough energy, it is possible to generate a current that flow through the device.

1.1 Types of Photodetectors

According to the operating mechanisms, photodetectors can be mainly classified as three different types: photoconductors, photovoltaic detectors, and photoemissive detectors [1].

Photoconductors are optical-sensitive elements, which responses to the light through changing its resistance or conductance. Figure 2 shows the geometry of a photoconductor.

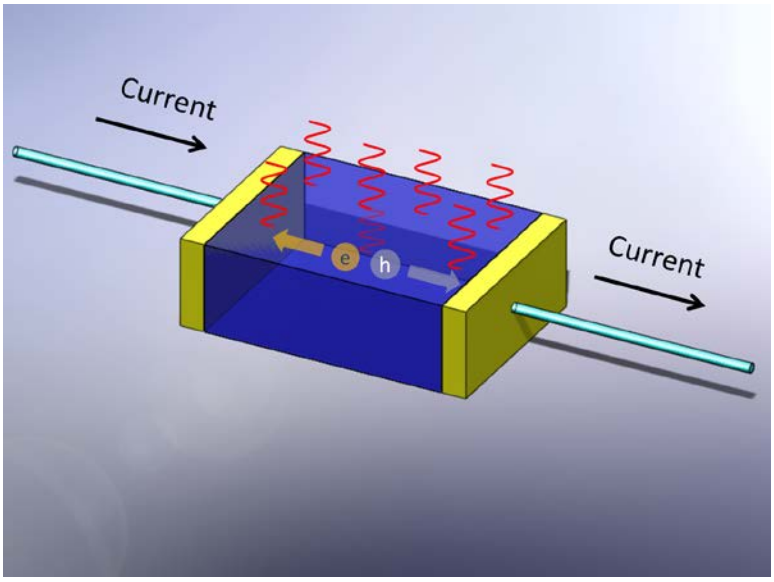

Figure 2: Photoconductor

Originally, the conductivity at thermal-equilibrium state is [2]:

$$\sigma_0 = e(\mu_n n_0 + \mu_p p_0) \tag{1.1}$$

Once the material absorbed the photon energy, excess carriers are generated inside the device, consequently, the conductivity increases to:

$$\sigma = e[\mu_n(n_0 + \delta n) + \mu_p(p_0 + \delta p)] \tag{1.2}$$

Where δn and δp are corresponding to the excess electrons and holes respectively. Compared with the initial state, conductivity increases by the mount of:

$$\Delta\sigma = e(\delta p)(\mu_n + \mu_p) \tag{1.3}$$

Photovoltaic detectors, also called photodiodes, operate by utilizing the rectifying characteristic of a p-n junction. A photodiode can produce a voltage or current response to the optical radiation under a reverse bias. [2]

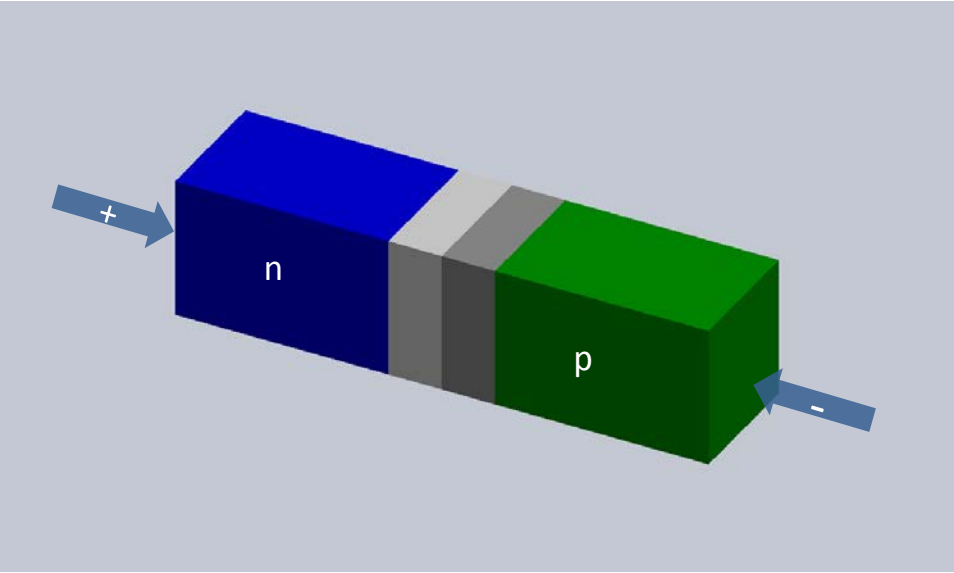

Figure 3a: Reverse-Biased Photodiode

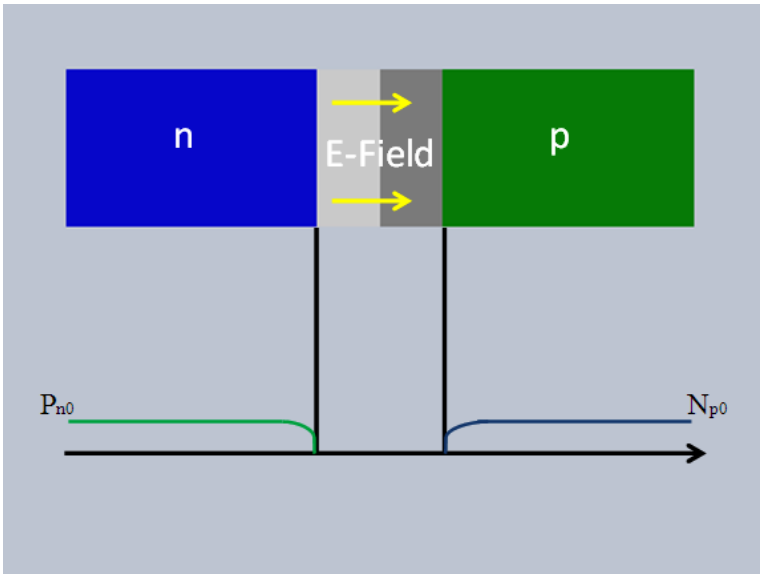

Figure 3b: Minority Carrier Distribution before Light Illumination

Figure 3a shows the reverse-biased diode and Figure 3b shows the minority carrier distribution in the reverse-biased junction prior to light illumination.

Photons enter from the top surface and pass through the p-type material (thin enough, the absorption can be neglect), absorbed in the space charge region then give rise to the electron-hole pairs. Immediately, the excess carriers generated by the light-matter interaction were swept out of the depletion region, electrons were drifted to n region, while holes flow toward p region. Photocurrent density can be described as below [1]:

$$J_{L1} = e \int G_L dx \tag{1.4}$$

Photoemissive detector, unlike the photovoltaic and photoconductor detectors, these detectors can work with an external photoelectron emission, which means that the photo-generated current is no longer flowing inside the device, but move in the external field. An energetic electron is capable of overcoming the work function of the material, as long as it gets sufficient kinetic energy from the photon. Once it jumps out of the surface and travels in the vacuum, the external electric field will pull it to the electrode, therefore, counted as an increase of the current. Figure 4 (E. L. Dereniak, 1996)[1] shows the working process of a photoemissive detector.

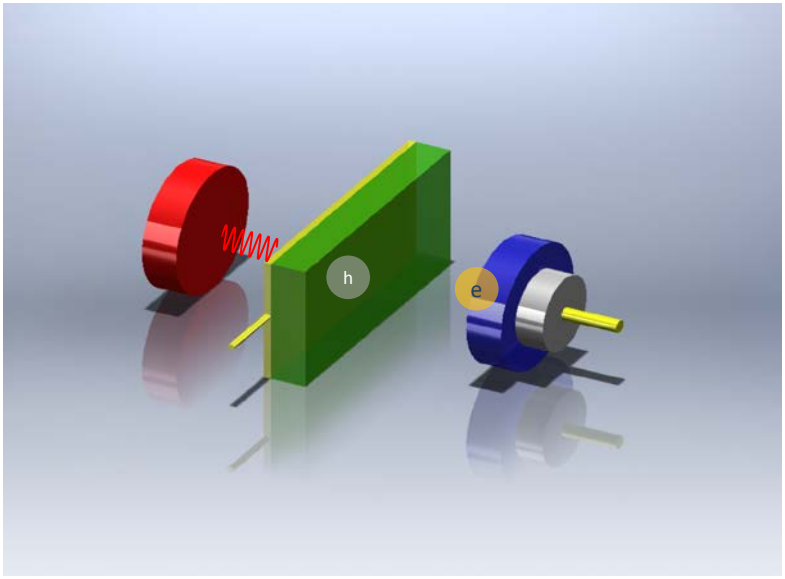

Figure 4: Photoemissive Detector

1.2 Quantum Dot Infrared Photodetectors

Infrared sensing and detecting technology has been widely used in both military and civil constructions [3], including night version, missile tracking and environmental monitoring. As monochromatic light moves further to the infrared region, traditional Interband Transition Photodetector fails to respond to the optical signal. The reason why it becomes transparent to the infrared light is that, photodetectors can only respond to the photons with energy equal or larger than the bandgap of the materials. When it comes to the infrared, photon energy is insufficient to excite an electron jumping over the bandgap. To match the special energy requirement, it is necessary to build up a bandgap engineered photodetector.

Quantum Dot Infrared Photodetectors (QDIPs) are well-developed semiconductor devices. Due to their 3D quantum confinement of the Quantum Dots (QDs) [4], QDIPs possess several prominent characteristics. A few advantages of these devices are: capability of detection of the normal incident light[3], reduced dependence of the carrier distribution on the temperature, higher photoconductive gain, carrier lifetimes 10-100 times longer than Quantum Well Infrared Photodetectors (QWIPs), and giving rise to a lower dark current. All these advantages make it surpass Quantum Well Infrared Photodetectors (QWIPs) [5].

1.2.1 Properties of a QDs

The most important characteristic of a QD proved to be its three dimensional confinement of the carriers [3]. Compared with a quantum well, the additional two confinements removes the rest degrees of freedom for the carrier, hence introduces some interesting properties of the QD. For simplicity, let's start with the quantum well then move on to a quantum box.

Three dimensional confinement

A one dimensional confinement has been applied in z direction, as illustrated by Figure 5.

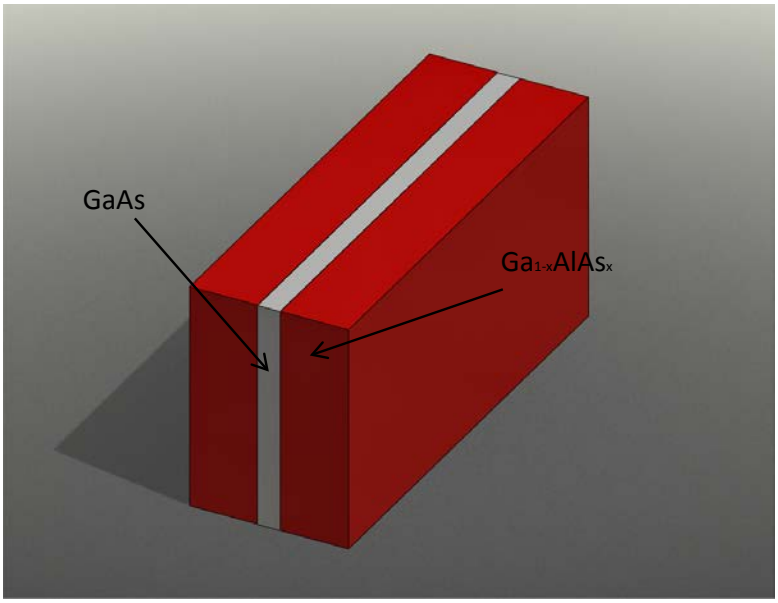

Figure 5: A Quantum Well made by GaAs and AlGaAs

Therefore, the Schrödinger's equation can be derived as [6]:

$$-\frac{\hbar^2}{2m}\left(\frac{\partial^2}{\partial x^2}+\frac{\partial^2}{\partial y^2}+\frac{\partial^2}{\partial z^2}\right)\varphi + V(z)\varphi = E\varphi \qquad (1.5)$$

The eigenfunction can be written as:

$$\varphi(x,y,z) = \varphi_x(x)\varphi_y(y)\varphi_z(z) \tag{1.6}$$

Substitute $\varphi(x,y,z)$ into (1.5), then we obtained:

$$-\frac{\bar{h}^2}{2m}\frac{\partial^2\varphi_x}{\partial x^2} = E_x\varphi_x \tag{1.7a}$$

$$-\frac{\bar{h}^2}{2m}\frac{\partial^2\varphi_y}{\partial y^2} = E_y\varphi_y \tag{1.7b}$$

$$-\frac{\bar{h}^2}{2m}\frac{\partial^2\varphi_z}{\partial z^2} + V(z)\varphi_z = E_z\varphi_z \tag{1.7c}$$

For (1.7a) and (1.7b), there is no confinement in x and y direction, see Figure 6.

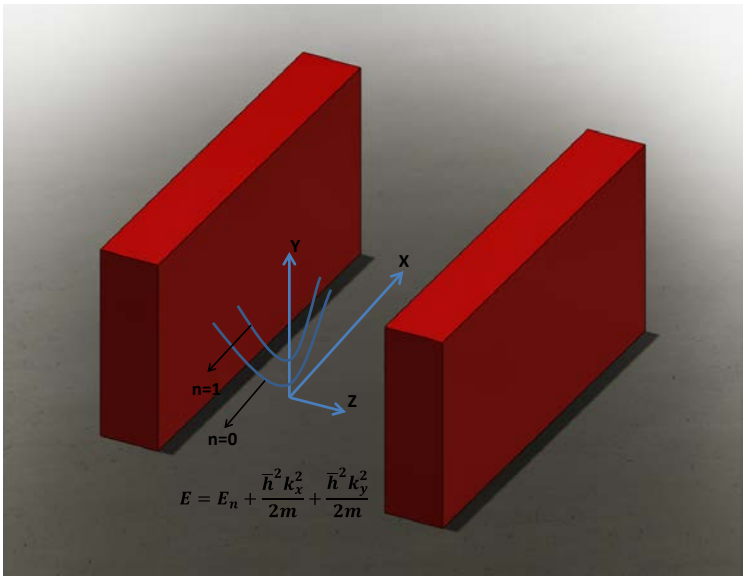

Figure 6: Dispersion Curve of Quantum Well in x and y Direction

So the eigenfunction should be in the form of a traveling wave, like:exp $(ik_x x)$ andexp $(ik_y y)$, thus:

$$-\frac{\bar{h}^2}{2m}\frac{\partial^2}{\partial x^2}\exp(ik_x x) = E_x\exp(ik_x x) \tag{1.8}$$

$$\frac{\bar{h}^2 k_x^2}{2m} = E_x \tag{1.9}$$

And the solution for the one dimensional confined axis is

$$E_z = E_n = \frac{\bar{h}^2\pi^2 n^2}{2mL_z^2} \tag{1.10}$$

Totally, the energy within a quantum well is [6]:

$$E = E_n + \frac{\bar{h}^2 k_x^2}{2m} + \frac{\bar{h}^2 k_y^2}{2m} \tag{1.11}$$

When it comes to a quantum box with dimensionsL_x, L_y and L_z, the wave function and energy states will change respectively, for the conduction band:

$$\varphi_{n,l,m} = \left(\frac{2}{L}\right)^{3/2} \sin\left(\frac{n\pi}{L_x}x\right) \sin\left(\frac{n\pi}{L_y}y\right) \sin\left(\frac{n\pi}{L_z}z\right) \tag{1.12}$$

$$E = E_c + \frac{\bar{h}^2\pi^2}{2m_c^* L_x^2} n^2 + \frac{\bar{h}^2\pi^2}{2m_c^* L_y^2} l^2 + \frac{\bar{h}^2\pi^2}{2m_c^* L_z^2} m^2 \tag{1.13}$$

where m_c^* is the effective mass of the electron in the conduction band.

Initially, electron energy state in conduction band is continuum, when the 3-D quantum confinement is induced; the conduction band splits into discrete energy levels.

Density of State (DOS)

Density of state is the number of states per energy per unit volume in real space.

$$\rho(E) = \frac{dN}{dE} = \frac{dN}{dk}\frac{dk}{dE} \tag{1.14}$$

For a quantum well [6],

$$N^{QW} = 2\pi k^2 \frac{1}{(2\pi/L)^2}\frac{1}{L^2} \tag{1.15}$$

$$\frac{dN^{QW}}{dk} = \frac{k}{\pi} \tag{1.16}$$

$$\frac{dk}{dE} = \frac{m^*}{k\bar{h}^2} \tag{1.17}$$

$$\rho^{QW}(E) = \frac{dN}{dE} = \frac{dN}{dk}\frac{dk}{dE} = \frac{k}{\pi}\frac{m^*}{k\bar{h}^2} = \frac{m^*}{\pi\bar{h}^2} \tag{1.18}$$

When there are more than one confined states in the quantum well, the total density of states are:

$$\rho^{QW}(E) = \sum_{i=1}^{n} \frac{m^*}{\pi\hbar^2} \vartheta(E - E_i) \tag{1.19}$$

where ϑ is the unit step function. Figure 7 gives an example of the density of states for bulk, Quantum Well and Quantum Dot.

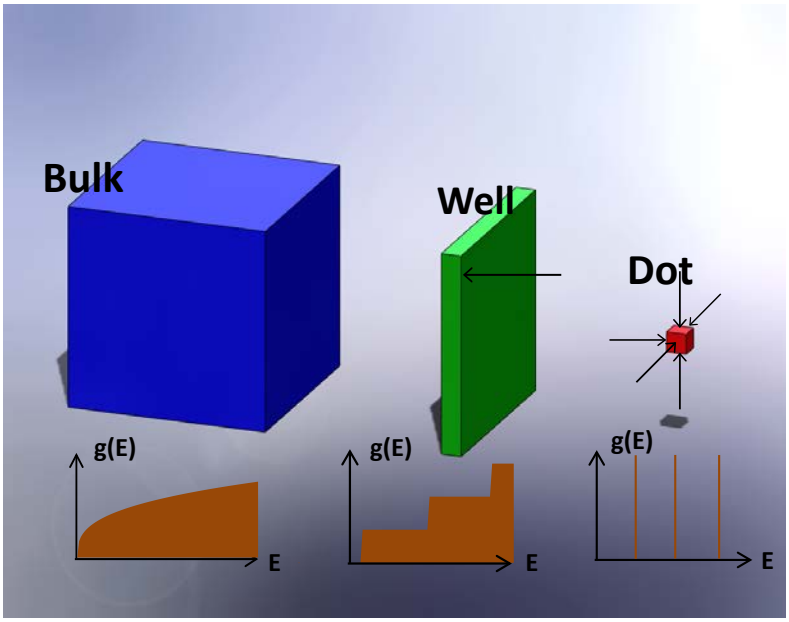

Figure 7: Density of State for Bulk, Quantum Well, and Quantum Dot

For the case of a QD, situation is quite different. Due to the zero-degree freedom, electrons were completely confined within the box, which means there is no dispersion curve. Under this circumstance, the density of state only depends on the number of discrete energy levels. Consequently, the DOS of a QD evolves into the form like a delta-function,

$$\rho^{QD}(E) = g(E_n)\delta(E - E_n) \tag{1.20}$$

where $g(E_n)$ is the degeneracy of the energy level E_n.

1.2.2 Advantages of QDIPs

Sensitivity to Normal-Incident Radiation

One of the advantages that the QDIP outperforms the QWIP is the capability of normal incident sensing. According to Fermi's Golden Rule, the rate of transition can be described as the probability from an initial state to a set of final states [7].

$$P_{in} = \sum_n P(i \to n) = g(E_1)P(i \to 1) + g(E_2)P(i \to 2) + \tag{1.21}$$

Where $P(i \rightarrow n)$ is the probability of transition from the initial state to the final state. Due to the transition selection rule, under the normal incident light, transition rate is zero for QWIP, since there is no confined state. Figure 8a and Figure 8b show the schematic view of a light incident on the surface of a quantum well with different angles. We can tell that the normal incident light is unable to provide the confinement in the direction where the E-Field oscillates.

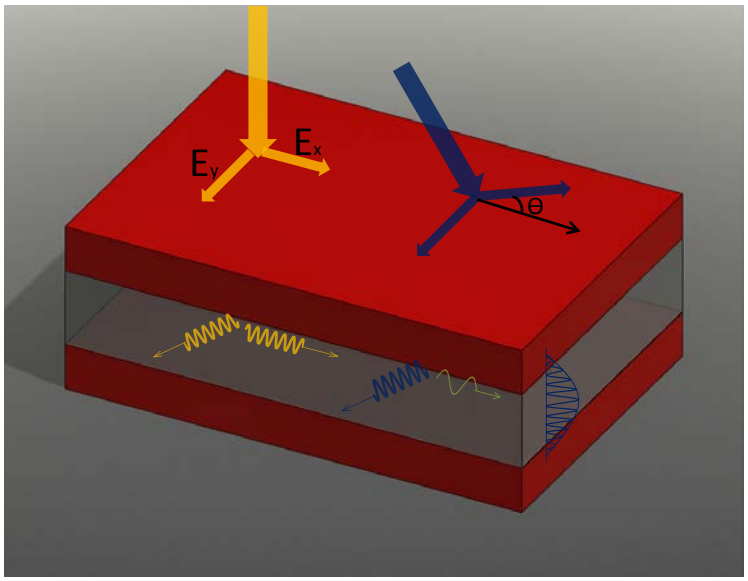

Figure 8a: Schematic View (3D) of Incident Light on a Quantum Well with Different Angle

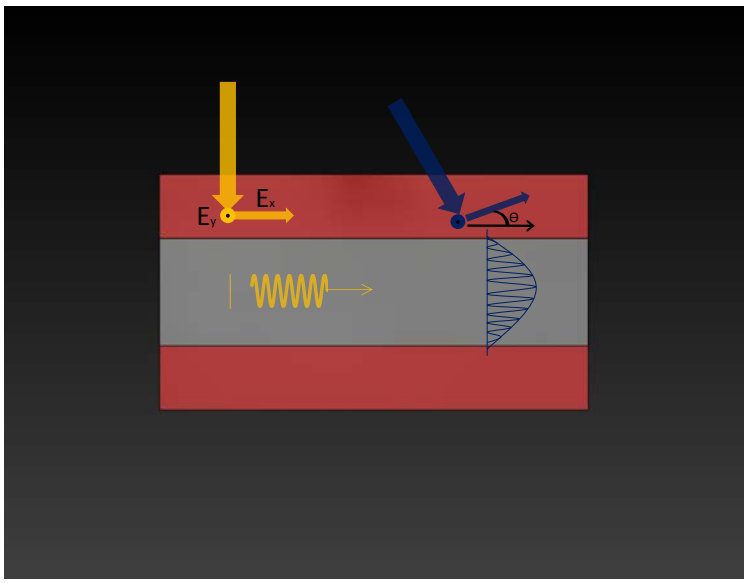

Figure 8b: Schematic View (side) of Incident Light on a Quantum Well with Different Angle

Let's take the two energy level electron system as a simple example. E_1 andE_2, correspond to the wave function $|\varphi_1\rangle$ and $|\varphi_2\rangle$ respectively. The incident light is perpendicular to the plane, and has an electric field E_x along x-axis. It is an "electric dipole" interaction between the photon and the electron [7]. In this case, the electron's energy will change when it has a displacement$x$, and the electric dipole momentum is$\hat{\mu} = -ex$, thus, the perturbing Hamiltonian will be [7]:

$$\widehat{H}_p = eE_x = -E_x\hat{\mu} \tag{1.22}$$

Where:

$$\mu_{mn} = -e\langle\varphi_m|x|\varphi_n\rangle \tag{1.23}$$

Using the quantized electromagnetic fields, Fermi's Golden Rule can be restated as [7]:

$$P_{mn} = \frac{2\pi}{\hbar}|\langle\varphi_m|-exE_x|\varphi_n\rangle|^2\delta(E_f - E_i) \tag{1.24}$$

Because:

$$\hat{\mu} = \begin{bmatrix}\mu_{11} & \mu_{12}\\ \mu_{21} & \mu_{22}\end{bmatrix} \tag{1.25}$$

If$\mu_{mn} = 0$, the probability will be equal to zero, which means it is impossible for the transition.

A quantum box processes the wave function: $|\varphi_m\rangle = \sin\left(\frac{m\pi}{L_x}x\right)$ in x-axis, therefore,

$$\mu_{mn} = -e\left\langle \sin\left(\frac{m\pi}{L_x}x\right)\middle|x\middle|\sin\left(\frac{n\pi}{L_x}x\right)\right\rangle \tag{1.26}$$

Due to the quantization in x direction, the normal incident light can be absorbed and detected by the QDIP. Figure 9 shows the lateral-confinement provided by the quantum dot.

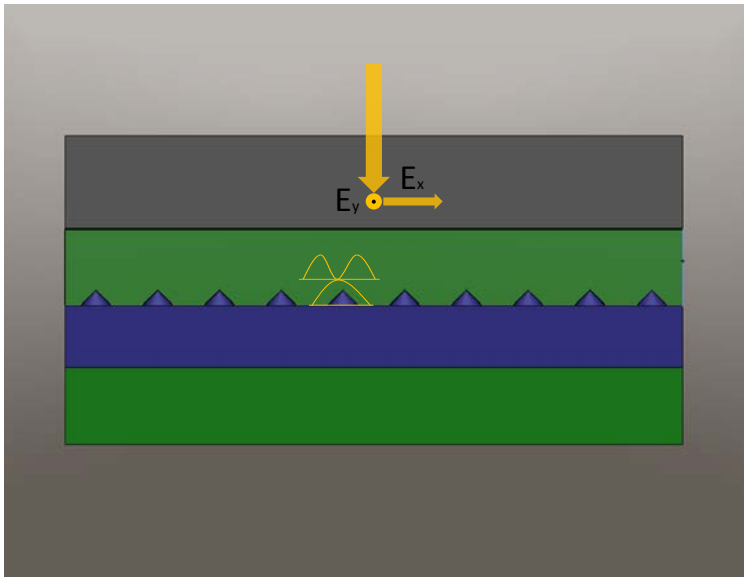

Figure 9: Lateral Confinement in a Pyramid-Like Quantum Dot

Lower Dark Current

The other attribute of QDIPs is the lower dark current. Electrons can be excited not only by incident photons, but also by the thermal excitation process. Thermally excited electrons are the major source of noise current in the detector as well.

At a stationary state (under zero bias), the thermal generation rate should be equal to the recombination rate. Without the applied electric field, the excited electrons cannot be swept out to form a current. They can go back to the bond state after a period ofτ.

$$R_{th} = R_{re} = \frac{N}{\tau} \tag{1.27}$$

Where *N* is the number of excited electrons and τ is the life time at the excited state.

When applying a high bias on the detector, the thermal-electrons can be sufficiently collected by the electrode before they relax to the ground state. In this case, all the thermal excited electrons can contribute to the current, which means:

$$qR_{th} = qR_{collect} = I = q\frac{N}{\tau} \tag{1.28}$$

Equation 1.28 shows the dark current is proportional to the ratio of excited electrons population over the carrier life time.

For a quantum well, the number of excited electrons is defined as:

$$N_{QW} = \int_{Em}^{\infty} \rho^{QW}(E)\, F(E) d(E) = \sum_m \int_{Em}^{\infty} \frac{m^*}{\pi \bar{h}^2} \vartheta(E - E_i) F(E) d(E) \tag{1.29}$$

For a QD,

$$N_{QD} = \rho^{QD}(E) F(E) = \sum_m g(E_n) \delta(E - E_n) F(E) \tag{1.30}$$

As we demonstrated before, the DOS for quantum dots are much less than quantum well, so the amount of thermal excited electrons in a quantum dot is largely reduced, which results in a lower dark current.

Higher Responsivity

For a photodetector device, the concept of responsivity has been developed as the ratio of electrical output over optical input [7]. (Figure 11 [5] Rosencher & Vinter) shows the geometry of a photoconductor.

Current density:

$$j_{ph} = \Delta n q \mu_n E = \frac{\eta \tau \phi_0}{d} q \mu_n E \tag{1.31}$$

photocurrent:

$$I_{ph} = j_{ph} w d = \eta q \mu_n \tau \frac{w}{l} \phi_0 V \tag{1.32}$$

responsivity:

$$R = \frac{I_{ph}}{P_{inc}} = \eta \frac{\mu_n \tau}{l^2} \frac{V}{h\nu / q} \tag{1.33}$$

Where τ is the excited carrier life time. Due to the Longitudinal Optical (LO) mode electron-phonon scattering process, carriers will relax to the ground state, subsequently, reduced the lift time. However, different from QWs, QDs have complete discrete energy levels, which make the electrons rarely achieved the interaction with LO phonon, thus effectively increases the life time. This phenomenon can be described by the following equation:

$$S_{eg} = \frac{2\pi}{\bar{h}} \left| \langle \varphi_e | -eV_{phonon} | \varphi_g \rangle \right|^2 \rho(E) \tag{1.34}$$

Where V_{phonon} is phonon-induced electrostatic potential, φ_e is the excited state, φ_g is the ground state, and $\rho(E)$ is the density of states. As discussed before, the density of states $\rho^{QD} \ll \rho^{QW}$ (see Figure. 7), thus the transition rate caused by the LO phonon are largely reduced in QDs, consequently, the carrier life time remains longer.

Based on the conclusion above, since the responsivity is proportional to τ, we can claim that QDIPs have a higher responsivity than QWIP.

2. Growth, Fabrication and Characterization

2.1 Growth Technology (MBE)

One of the most commonly used techniques to obtain Quantum Wells and Quantum Dots devices is Molecular Beam Epitaxy (MBE) [5]. Impinging a 'molecular beam' which contains a special material on to the substrate, MBE can create the crystal by depositing the atoms layer by layer. The atomic-level growth provide us a more accurate way to control the properties of our devices, in the meantime, slow deposition rate requires high vacuum level in order to keep a pure growth environment.

Self-assembled InAs quantum dots device is also grown by MBE using the Stranski-Krastanov method. After inducing a lattice mismatch between different materials such as InAs on GaAs, strains were accumulated [8]; when the thickness of the atom film reaches the critical value, the shape will be damaged and the edge dislocation will appear [5], in that way, a quantum dot is formed due to the inherent behavior of the material to relax stress.

2.2 Growth Condition and Process

The QD samples here are grown by using a V80H MBE system. At the first step, a 100 nm undoped GaAs buffer layer was formed right above the substrate, a semi-insulting GaAs (100) wafer; after that, a 0.3µm Si-doped (n^+) GaAs contact layer (n = $1\times10^{18}cm^{-3}$) was deposited on the buffer layer. The active region for our detector is formed by 10-25 periods of InAs quantum dots absorption layer with spacer layers of GaAs sandwiched in between. Each QD layer included 1 nm $In_{0.15}Ga_{0.85}As$ and 2 monolayers (ML) of InAs QDs, the thickness of GaAs spacer was 50 nm. The top contact layer was Si-doped (n=$1\times10^{18}cm^{-3}$) GaAs layer with the thickness of 0.1 µm.

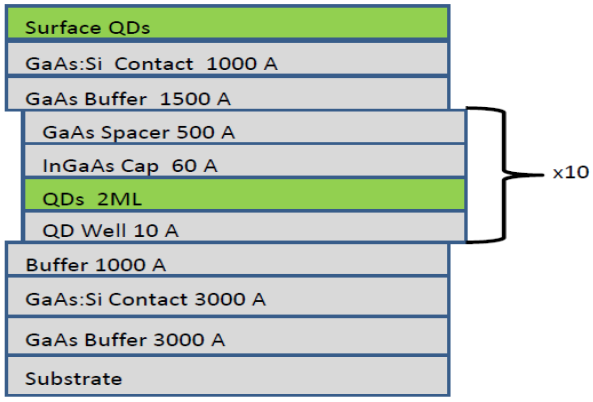

Figure 10: Sample Quantum Dot Growth

2.3 Fabrication

The fabrication process of Infrared Quantum Dot Photodetectors is schematically demonstrated in Figure 11a-j [5]:

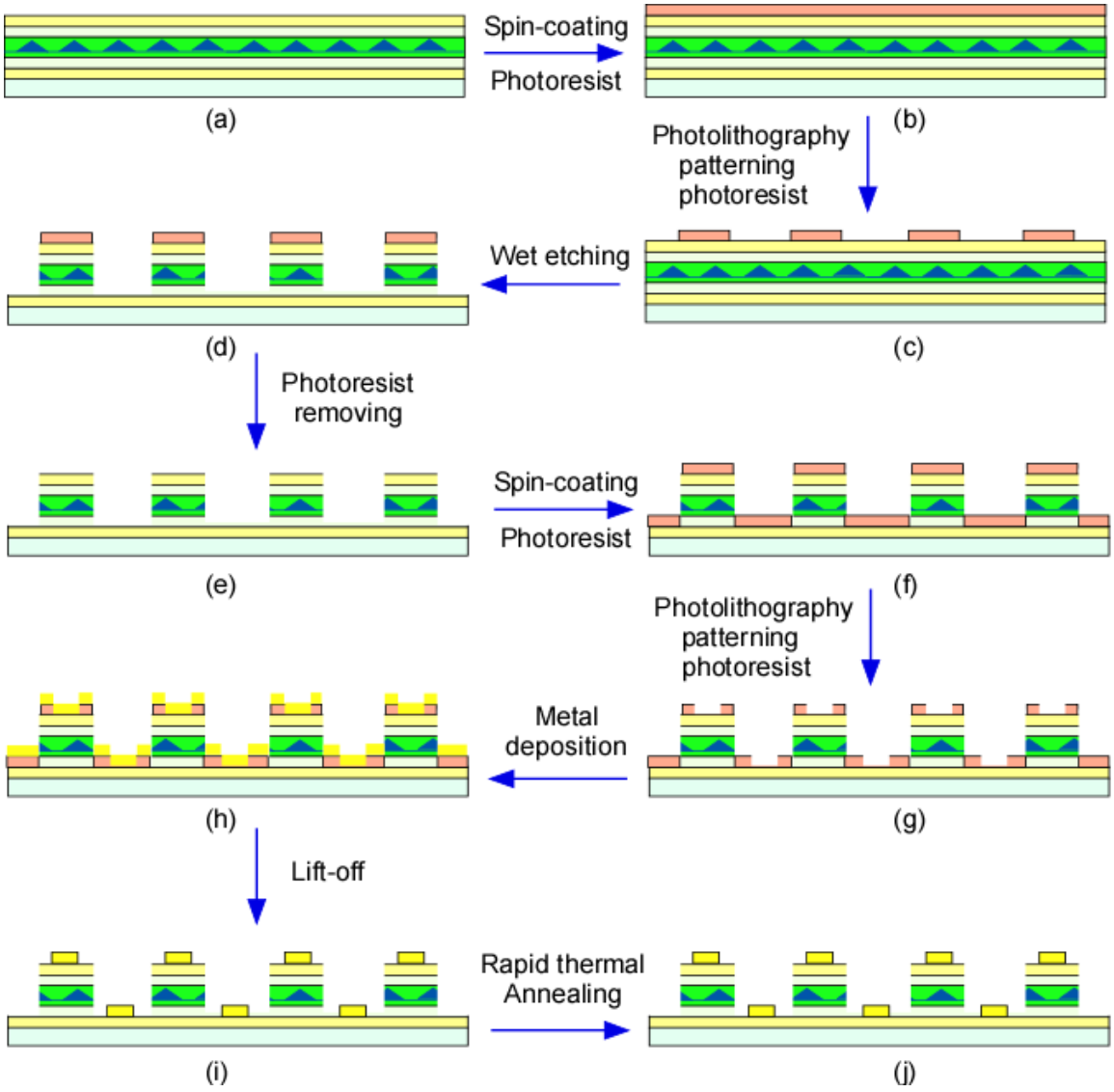

Figure 11a-j: Fabrication Process of QDIPs

After MBE growth, the photodetector array is fabricated using the steps shown above. The wafer is spin-coated with a positive photoresist. After 3 minutes soft baking at 95C°, the wafer is then exposed with ultraviolet (UV) light using a photo mask containing the QDIP patterns. The exposed wafer is then developed using CD-30 developer. The desired photoresist pattern will be transfer onto the wafer. The wafer is then etched by using the standard wet etching procedures, which is piranha etch solution contained sulfuric acid (H_2SO_4): hydrogen peroxide (H_2O_2): water (H_2O) in the ratio of 1: 8: 80 by volume.

The QDIP mesa will be formed. The photoresist is then removed using a solvent bath and the wafer is then washed using deionization (DI) water and spin coated with the photoresist and soft bake again. Using the mask for metal patterns, we aligned the photo mask with mesas and expose. After it is developed, the metal contact patterns on the wafer will be opened. The wafer is then deposited with the metal alloys (Ni 50Å /Ge 170Å /Au 330Å /Ni 150Å /Au 3000Å). The unwanted metals are lifted off by soaking in Acetone in the ultra-sonic bath and finally annealed. The sample is then wire-bonded and is ready to be tested (Figure 12).

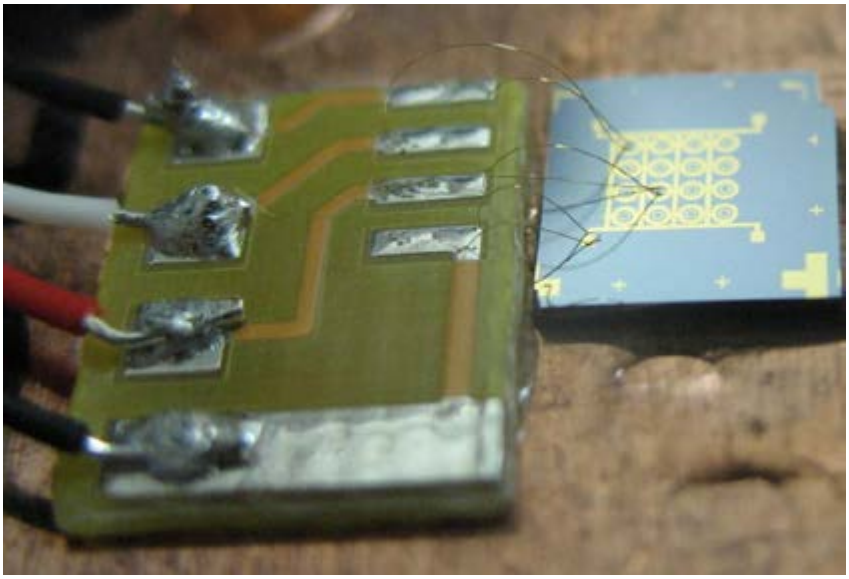

Figure 12: Wire Bonded Detector Ready to be Tested

2.4 Characterization

2.4.1 Spectral Response Measurement of QDIPs

Typically, the spectrum response of a standard QDIP is obtained by measuring the Fourier Transform Infrared (FTIR) spectrometer signal. Figure 13 shows the schematic view of a FTIR spectrometer. Blackbody source, 50% beam splitter, moving mirror, fixed mirror and an Infrared Photodetector are the main components of a typical FTIR spectrometer.

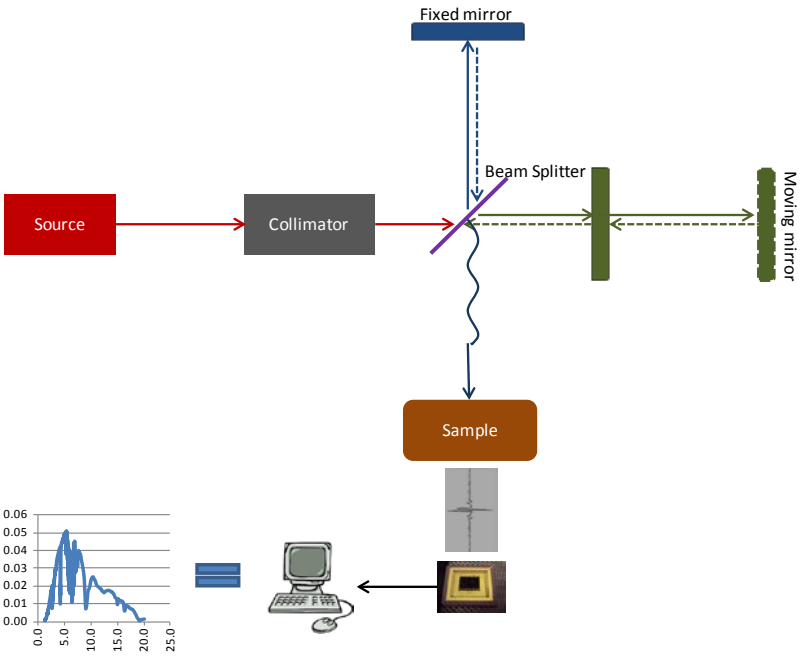

Figure 13: Schematic View of FTIR Spectrometer

During the operation of each scan, the beam splitter took the incoming infrared (IR) light and divided it into two paths, heading to the fixed and moving mirror respectively. The two reflected beam recombined when back to the splitter and passed through a sample. Due to the constantly changed optical path difference induced by the moving mirror, the two beams interfered with each other and consequently generated an interferogram. Different from the normal optical or UV spectrometer, each point of the FTIR interferogram contained all the frequency information from the blackbody source. The interference of those two beams can be described as below:

$$I(x) = |E_1 + E_2|^2 = E_1^2 + E_2^2 + 2E_1E_2\cos(\delta) = \frac{I_0}{2} + \frac{I_0}{2}\cos\left(\frac{2\pi}{\lambda}x\right) \tag{2.1}$$

where I_0 is the intensity of the incident light, x is the optical path difference induced by the moving mirror and λ is the wavelength. The $I(x)$ can also be expressed as:

$$I(x) = \int_0^{\infty} \frac{I_0}{2}\left[1 + \cos\left(\frac{2\pi}{\lambda}x\right)\right] G(\lambda)d\lambda \tag{2.2}$$

In equation (2.2), $G(\lambda_0)$ is actually the transmission performance of the sample at a specific wavelengthλ_0. If we take the reverse Fourier Transform of the AC part from (2.2), the transmission profile will be obtained:

$$G(\lambda) = \int_{-\infty}^{+\infty} I(x)\exp\left(-j\left(\frac{2\pi}{\lambda}x\right)\right)dx \tag{2.3}$$

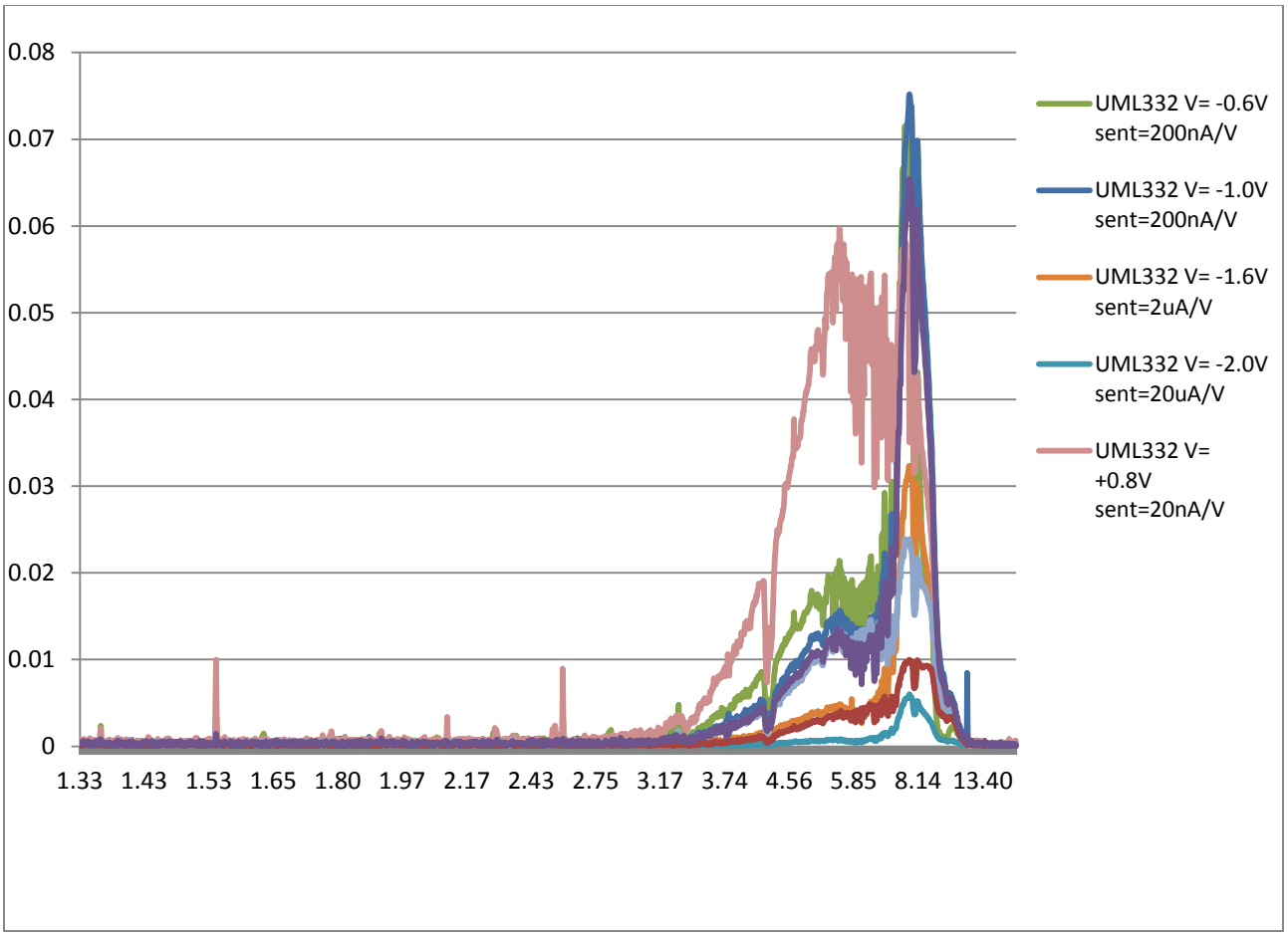

Figure 14: Transmission Response in Arbitrary Units
QDIP versus wavelength in micron for sample UML-332 under different voltage biases

By replacing the internal IR detector with the QDIPs, the spectral response of our device can be measured with the assistant of external pre-amplifier. The schematic set up diagram is demonstrated in Figure 15. At first, the sample was mounted into the cryo-chamber (Janis, model ST-100) and connected to the outside circuit which applied voltage on the sample. Then the chamber was inserted into the FTIR body (Bruker, Tensor27), IR beam had been aligned on the mesa surface afterward. Bias voltage was provided by pre-amplifier (Standford research systems, model SR770), operating temperature was well controlled by the temperature controller (Lakeshore, 331 Temperature Controller) connects to the chamber to adjust temperature.

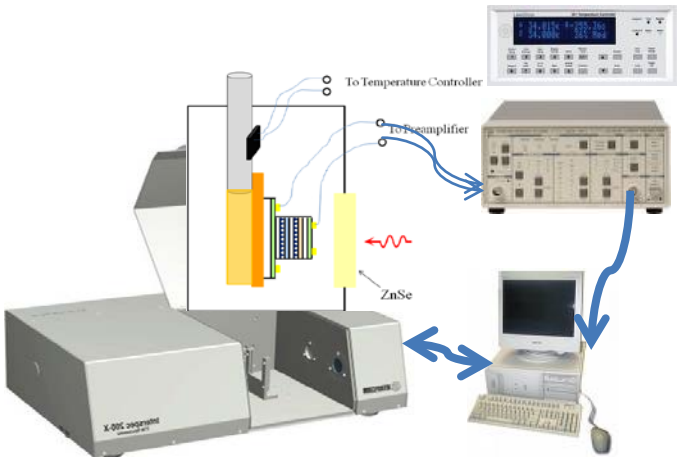

Figure 15: Schematic Diagram of Spectral Response Testing Setup for QDIPs

2.4.2 Photocurrent Measurement of QDIPs

Photocurrent is the current in the IR detector that responses to the black body radiation. Once the active material absorbed the photon energy, excess carriers are generated inside the device and the overall conductivity has been increased. As a result, an extra amount of current flows through the device, which is the photocurrent.

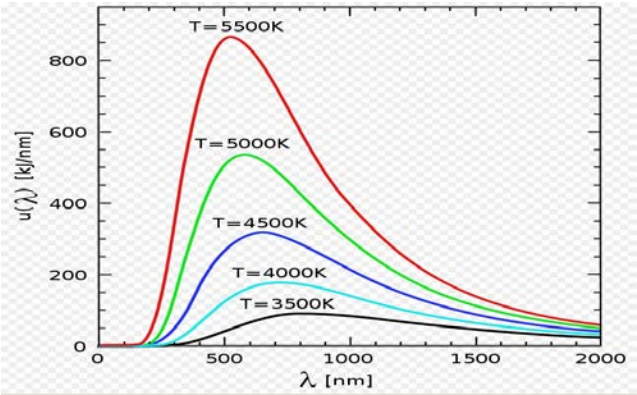

Figure 16: Black Body Radiations at Different Temperatures

During the measurement of photocurrent signal, a blackbody radiation was placed in front of the chamber, which worked as the light source and emitted infrared light. An external chopper was mounted between the radiation source and the chamber, to modulate the incident light at frequency between 590 and 600Hz. Bandpass optical filters (2.4µm, 3.6 µm, 4.5 µm, 7 µm) were also placed in front of the ZnSe window of the cryo-chamber, to restrict the incident radiation to the wavelengths of interest. To measure the photocurrent a Stanford Research SR760 spectrum Fast Fourier Transform (FFT) analyzer was used. A preamplifier was inserted between the QDIP, to increases the signal of the

photocurrent and bias the QDIP and the measured photocurrent was modulated at 593 Hz to avoid the 1/f noise.

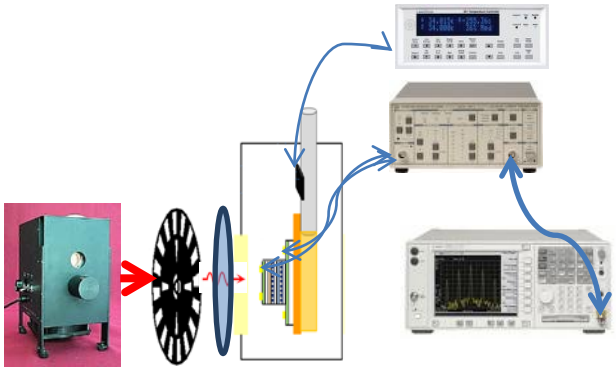

Figure 17: Photocurrent Test set up in the Lab

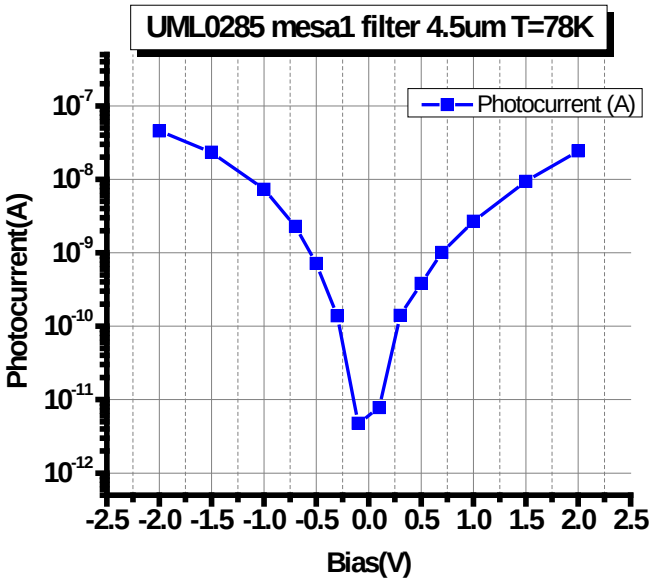

Figure 18: Photocurrent Tested for Sample UML0285

Figure 18 shows the photocurrent of a QDIP tested by the system. The bandpass filter was 4.5µm, operating temperature was 77K, blackbody radiation emitted at 1000K, chopper modulated as 593Hz.

2.4.3 Dark Current and Noise Current Measurement of QDIPs

As the main source of noises in an IR detector is dark current. Dark current has a great impact on the performance of the QDIPs. The dark current is measured eliminating the IR and visible radiation incident on the QDIP and measuring the reverse biased current (I) and voltage (V) relationship of the QDIP. The window of the cryo-chamber was cover with Aluminum foil to eliminate the incident

radiation and the QDIP was cooled down to 77K. The I-V measurements were performed with a Keithley 2602 sourcemeter, which varied the bias voltage and measured the current. As shown in Figure 19 the I-V curve was generated by plotting each data point of the current-voltage pair.

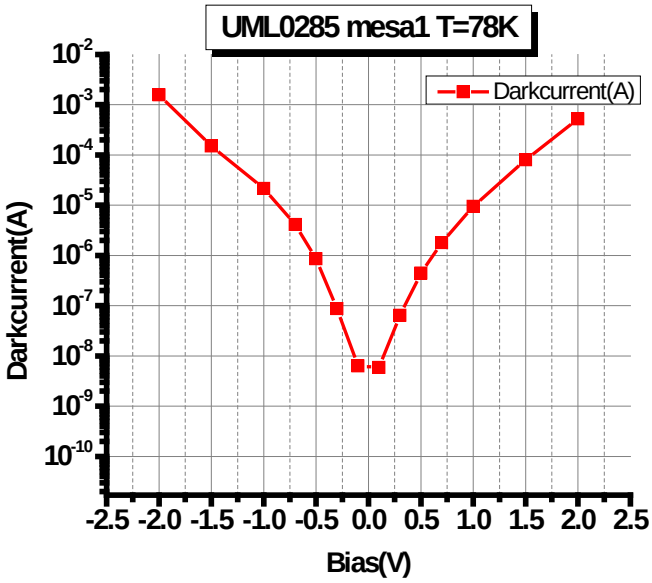

Figure 19: Dark Current of QDIPs Measured by Source Meter

Noise current is defined as the spectral density of dark current, in order to measure this parameter, a FFT spectrum analyzer and preamplifier replaced the Keithley sourcemeter . The cryo chamber was kept 77K and the QDIP was shielded from the incident light. The schematic view of the noise current setup is shown in Figure 20.

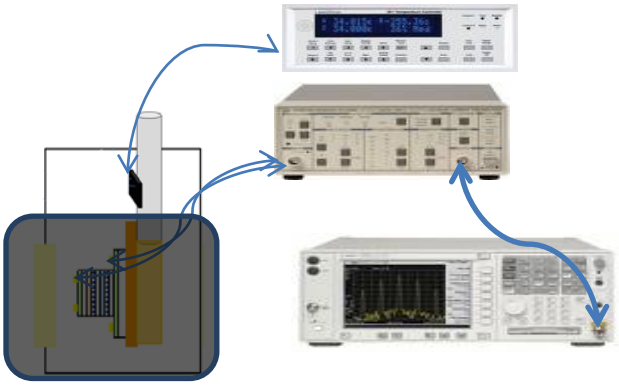

Figure 20: Schematic View of Noise Current Setup

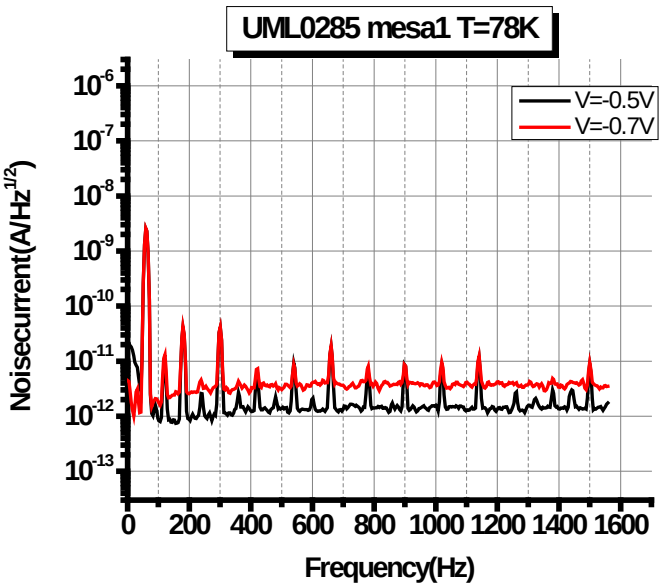

Figure 21: Dark Current Spectrum under Different Voltage Biases

Figure 21 shows the dark current spectrum under different bias voltage And the 1/f noise is dominate at low frequencies. T As seen in Figure 21 the 1/f noise is minimized at frequencies ≥ 593 Hz and the noise current is less than 2 x 10^{-10} A/$Hz^{1/2}$.

3. References

[1] Dereniak, E. L. and Boreman, G. D., “Infrared Detectors and Systems”, Wiley, 1996.

[2] Neaman, D. A., “Semiconductor Physics and Devices”, McGraw-Hill Science, 2002.

[3] Campbell, J.C. and Madhukar, A., “Quantum-Dot Infrared Photodetectors”, Proceedings of the IEEE, vol. 95, pp. 1815-1827, 2007.

[4] Liu, H. C., “Quantum Dot Infrared Photodetector”, Opto-Electron. Rev., vol. 11, pp. 1-6, 2003.

[5] Vasinajindakaw, P., Master’s thesis, “Verification and Reduction of Dark Current on Quantum Dot Infrared Photodetector”, Electrical and Computer Engineering Department, University of Massachusetts at Lowell, 2009.

[6] Harrison, P., “Quantum Wells, Wires, and Dots”, John Wiley & Sons, 2005.

[7] Rosencher, E. and Vinter, B., “Optoelectronics”, Cambridge University Press, 2002.

[8] Vaillancourt, J., Master’s thesis, “A Multispectral Quantum Dot Infrared Photodetector”, Electrical and Computer Engineering Department, University of Massachusetts at Lowell, November 2007.

LIST OF ACRONYMS, ABBREVIATIONS, AND SYMBOLS

ACRONYM	DESCRIPTION
DI	Deionization
DOS	Density of State
FFT	Fast Fourier Transform
FTIR	Fourier Transform Infrared
IR	Infrared
LO	Longitudinal Optical
MBE	Molecular Beam Epitaxy
ML	Monolayer
QD	Quantum Dot
QDIP	Quantum Dot Infrared Photodetectors
QW	Quantum Well
QWIP	Quantum Well Infrared Photodetectors
UV	Ultraviolet